Simultaneous Inversion of cross-dipole acoustic waveforms in anisotropic media for azimuthal angle and dispersion of fast and slow shear waves

Victoria Briggs, Rama Rao V.N., Daniel R Burns.
Earth Resources Laboratory
Dept. of Earth, Atmospheric, and Planetary Sciences
Massachusetts Institute of Technology
Cambridge, MA 02139

Abstract

A method to jointly invert for azimuthal angle and dispersion relations from cross-dipole data is presented. Dispersion curves from the joint inversion are compared to both Prony's method and a simple back propagation schema and an agrrement is found. The azimuthal angle estimate is shown to differ from a frequency domain rotaion that takes no account of dispersion within the waveforms indicating the importance of joint inversion.

1 Introduction

Spatial ordering on a scale smaller than the investigating wavelength will be seen as anisotropy by a cross-dipole acoustic borehole tool. The anisotropy can be intrinsic to the formation as caused by crystal structure, grain orientation, or micro cracks, or it can be extrinsic due to fractures, faults, stress, or bedding planes. The alignment of these phenomena causes a directionally preferential stiffness, which causes directionally dependent velocities. Either form of anisotropy can cause shear wave splitting, which is the polarization of the vertical and horizontal shear waves into their fast and slow components. Anisotropy information can be used to calculate fracture orientation (Tichelaar and Hatchell (1997)) and fracture density (Tatham et al. (1992)). Combining azimuth and the dispersion information it is possible to calculate 'in-situ' stress fields (Huang (1998)) and (Sinha and Kostek (1996)), which, if present, is necessary information for optimization of well placement and production.

In the low frequency regime, cross-dipole acoustic tools excite the lowest order dipole mode known as the flexural mode. The flexural mode is the motion of the borehole 'flexing' from side to side in the formation, and the flexural wave is a guided mode which travels along the borehole-formation interface. This dipersive mode assymptotes to the shear velocity at low frequencies and the stoneley wave velocity at high frequencies (Kurkijian and Chan (1986)). In a transversly anisotropic formation, the borehole flexural mode dispersion is sensitive to radial position, and can therefore be used to calculate anisotropy (Sinha et al. (1994)). If the waveforms are not corrected for dispersive effects, velocity processing such as semblance can lead to erroneous results (Kimball (1998)).

In this paper we present a method to invert cross-dipole data for azimuthal angle of anisotropy with respect to the dipole tool axis and for the dispersion curves of the fast and slow shear waves simultaneously. Current processing does each of these steps individually: first the recorded wave forms are projected onto the fast and slow axes to find the azimuthal angle and then the fast and slow wave components are processed seperately for shear wave velocities. If the mode is undispersive, Alford rotation (Alford (1986)) can be used to project the waveforms onto the fast and slow shear mode components. Dispersion of the flexural mode is a function of the geometry of the borehole, the formation, and the fluid parameters. Although the cross-diopole tool excites waves in the low frequency regime, there can be substantial dispersion (Tang

et al. (1995)). Thus, any rotation scheme that does not consider dispersion in the waveforms may produce eroneous results (Huang et al. (1998)).

Tang and Chunduru (1999) et al have shown the feasibility of combining this two-step process into a one-step inversion, using the cross-dipole waveforms to find azimuthal angle and shear wave velocities. The work presented here follows a similar methodology but inverts for the full dispersion curves as well as the azimuth.

2 The Objective function and Inversion Method

(Please refer to appendix for a detailed discussion on cross-dipole data.)
To set up this problem as an inversion, it is necessary to form an objective function whose minimum corresponds to the correct values of the paramaters being inverted for. (ie $v_f(\omega)$, $v_s(\omega)$ and θ). If the two inversions for azimuth and phase velocities are performed separately, the second inversion result is conditional on the first. This conditionality means that any error in the first result will be carried into the second. Performing a joint inversion gives the global best estimate for all of the parameters simultaneously and provides an unconditional result.

We know that for the correct azimuth, θ, the back rotated signals $f_n(\omega)$ and $s_n(\omega)$ will be maximized. We can therfore find the derivative of equations 15 and 16 and set it to zero (or minimize, in the case of an inversion) to obtain the azimuthal angle,

$$\frac{\partial f_n(\omega)}{\partial \theta} = (yy_n - xx_n)\sin 2\theta + (xy_n + yx_n)\cos 2\theta = 0 \tag{1}$$

$$\frac{\partial s_m(\omega)}{\partial \theta} = (xx_m - yy_m)\sin 2\theta - (xy_m + yx_m)\cos 2\theta = 0 \tag{2}$$

where n and m refer to the receiver number for the fast and slow arrays, respectively. Because both $\frac{\partial f_n}{\partial \theta}(\omega)$ and $\frac{\partial s_m}{\partial \theta}(\omega)$ would ideally be zero independently, for the correct azimuth, their difference $\frac{\partial f_n}{\partial \theta}(\omega) - \frac{\partial s_m}{\partial \theta}(\omega)$ also vanishes. In order to have an objective function that is also sensitive to correlations in the data (i.e. between receivers), we chose to minimize the quantity $\int d\omega \left|\frac{\partial f_n}{\partial \theta}(\omega) - \frac{\partial s_m}{\partial \theta}(\omega)\right|^2$. Note also that when the signal is incorrectly back-rotated, the f_n and s_n data both contain fast and slow components which are correlated and correctly picked-up by such an objective function.

For the propagation, we know that if the correct velocity was used at each frequency, the data at each receiver will be back propagated to the source function. Thus if we undo the propagation correctly and subtract the signal from any receiver pair the absolute value of their difference should vanish.

Therefore, our choice for an objective funtion is

$$O[v_f(\omega), v_s(\omega), \theta] = \int_\omega \sum_{n,m} \left|\frac{\partial f_n(\omega)}{\partial \theta} - \frac{\partial s_m(\omega)}{\partial \theta}\right|^2 + |f_n(\omega) - s_m(\omega)|^2 . \tag{3}$$

which is sensitive to both azimuth angle and fast and slow dispersion. In addition, this objective function combines all the data from all receivers, and its minimization should therefore enable one to obtain the best fitting parameters (azimuth as well as fast and slow mode dispersion curves) taking into account the maximum amount of information contained in the data. This method is to be contrasted with more traditional methods (for example, first estimate the azimuth independently of dispersion and then seperately analyze the fast and slow mode data), that only partially take into account all the information contained in the data. Equation 4 is another representation of 3, it shows in matrix form how the inversion calculates the value of the objective function for the trial functions v_{s-t}, v_{f-t} and θ_{trial} for a receiver spaced a distance z_n from the source

$$\begin{pmatrix} \frac{1}{2}e^{-\frac{iz_n\omega}{v_{f-t}(\omega)}}\left[e^{\frac{iz_n\omega}{v_f(\omega)}}+e^{\frac{iz_n\omega}{v_s(\omega)}}+\left(e^{\frac{iz_n\omega}{v_f(\omega)}}-e^{\frac{iz_n\omega}{v_s(\omega)}}\right)\cos 2(\theta-\theta_t)\right] & \\ \frac{1}{2}e^{-\frac{iz_n\omega}{v_{s-t}(\omega)}}\left[e^{\frac{iz_n\omega}{v_f(\omega)}}-e^{\frac{iz_n\omega}{v_s(\omega)}}\right]\sin 2(\theta-\theta_t) & \\ & \frac{1}{2}e^{-\frac{iz_n\omega}{v_{f-t}(\omega)}}\left[e^{\frac{iz_n\omega}{v_f(\omega)}}-e^{\frac{iz_n\omega}{v_s(\omega)}}\right]\sin 2(\theta-\theta_t) \\ \frac{1}{2}e^{-\frac{iz_n\omega}{v_{s-t}(\omega)}}\left[e^{\frac{iz_n\omega}{v_f(\omega)}}+e^{\frac{iz_n\omega}{v_s(\omega)}}+\left(-e^{\frac{iz_n\omega}{v_f(\omega)}}+e^{\frac{iz_n\omega}{v_s(\omega)}}\right)\cos 2(\theta-\theta_t)\right] & \end{pmatrix}. \tag{4}$$

One can see from inspection of 4 that if $\theta_t = \theta$, the two off diagonal terms will be zero and the diagonal terms will be maximized. If $v_{s-t} = v_s$ and $v_{f-t} = v_f$, the two diagonal terms will be zero but the off diagonal terms will still have a contribution unless the trial angle is correct. The full dispersion curve speciincr fies a velocity for each frequency component in the data. Depending on the size of the fourier transfom used to convert the data into the frequency domain, there can be a large number of parameters to invert for. Typically if the traces have 512 samples in time and a 512 fast fourier transform is performed, there will be 256 frequencies to invert for on each dispersion curve. This leads to an inversion search space of 513 parameters $(2 \times 256(frequencies) + 1(angle))$. In order to avoid inverting such a large model space the dispersion curves can be parametrized by using piecewise constants, for example. Essentially this divides the frequency space into a number of bands over which the dispersion curve is described by a constant. The inversion code implements a variable grid algorithm, which dynamically updates the placement and size of the frequency bands with each iteration. The algorithm has two stages. The first, known as the spinup, uses regularly spaced bins to estimate the rough form of the data's dispersion curve. At each spinup iteration the code doubles the number of piecewise constants it uses to fit the curve. At the first iteration it fits one constant which represents some average phase velocity; at the next iteration it fits two, and at the next 4, and so on. The spinup is typically run for 4 iterations, which means that the dispersion curve has been parametrized by 8 evenly spaced (in frequency) constants. These iterations provides the best possible starting guess for the second part of the algorithm which uses the variable spacing. After each minimization iteration the grid refining code allocates the number of frequency bins to be used acording to the shape of the dispersion curve at those frequencies. In other words, the algorithm adds more frequency bins where the gradient of the curve is largest, ensuring that the inversion has enough parameters to capture the character of the curve while keeping the number to a minimum so that the inversion runs efficiently. Figure 2 shows the objective function space for some synthetic flexural wave forms. The data was created using the dispersion relations and source spectrum shown in figure 1. The plots were made by dividing the frequency axis into 4 regions (shown as the red vertical dotted lines in 1) and holding three of the phase velocities constant, at the correct value, while varying the fourth. The objective function surface is shown for the low, mid-low, mid-high, and high regimes and the pink star marks the true minimum of the surface. Figure 4 shows a similar view of the surface as a function of aximuthal angle; here one of the dispersion curves is held at a constant while the angle and second dispersion relation are varied in the 4 frequency bins. These figures are shown to illustrate a few important results regarding the inversion. It is obvious from the number of minima in the plots that the objective function has a strong frequency dependence: as the frequency increases, so does the complexity of the surface. This is due to the phase wrap around between source and first receiver. Figures 3 and 5 show the inversion space when the initial offset is reduced to zero. The distance between each of the receivers is small compared to the shortest wavelength in the dipole data spectrum and thus there is no phase wrap around of the signal between receivers. However, between the source and the first receiver there is a large offset meaning the phase has gone through many cycles before reaching the first receiver. This can be calculted by considering the phase velocites of one of the modes in adjaccent minima and calculating the difference in phase between them. For example if we consider the minima at 3100 ms^{-1} (the true mode velocity) and the adjacent minima to the left at around 2800 ms^{-1} in the high end frequency block with average frequency $11kHz$. Using the middle receiver which is a distance 4.573m from the source we find a phase difference between the two minima of aproximately 2π radians. Back propagation to the source is therefore difficult because it involves unwrapping this large phase exactly. A small error in the velocity can result in a change of this phase by 2π, thus leading to a local minimum in the objective function.

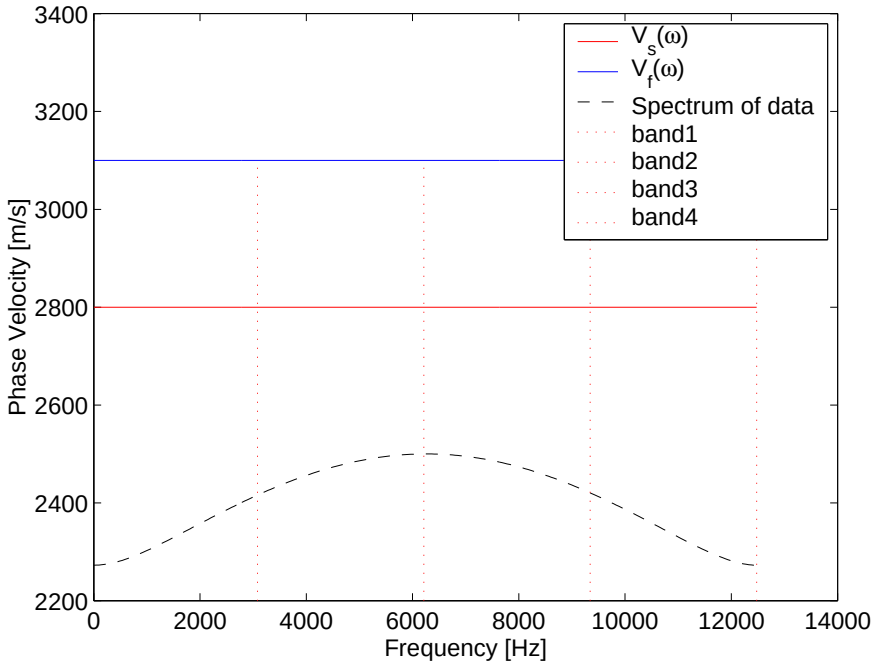

Figure 1: Dispersion Relations for fast and slow modes and the spectrum of synthetic data used for objective function surfaces.

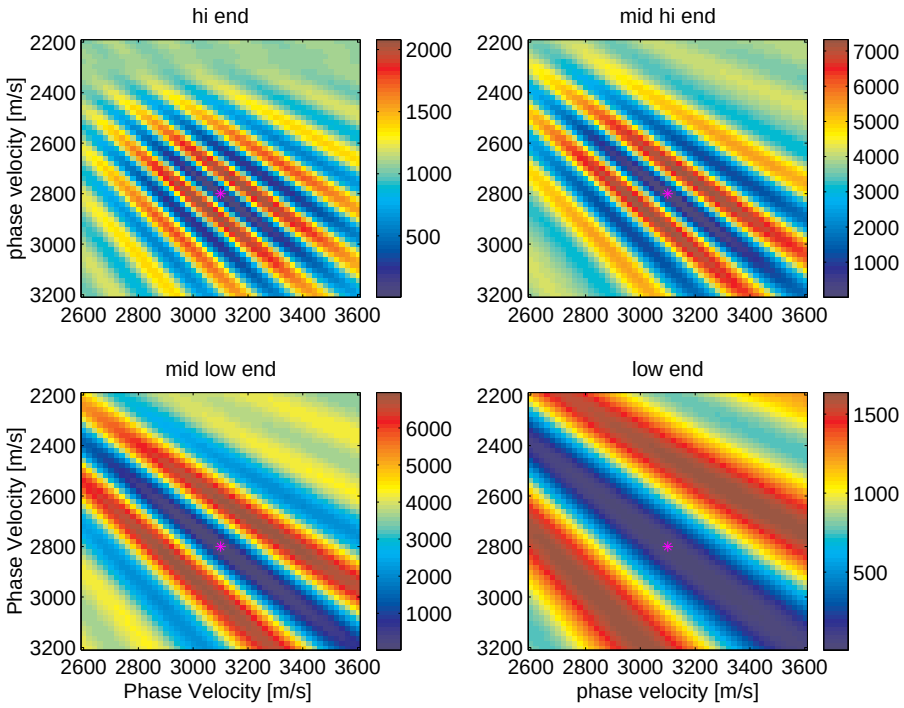

Figure 2: Objective function surfaces for 4 different frequency bands and the correct rotation angle.

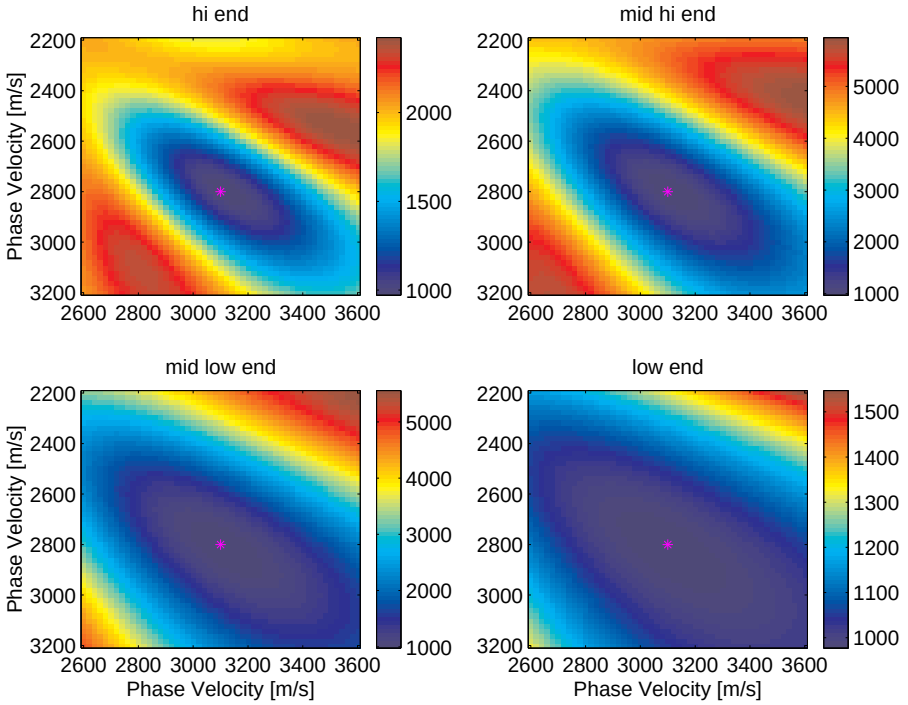

Figure 3: Objective function surfaces for 4 different frequency bands and the correct rotation angle with zero offset to first receiver.

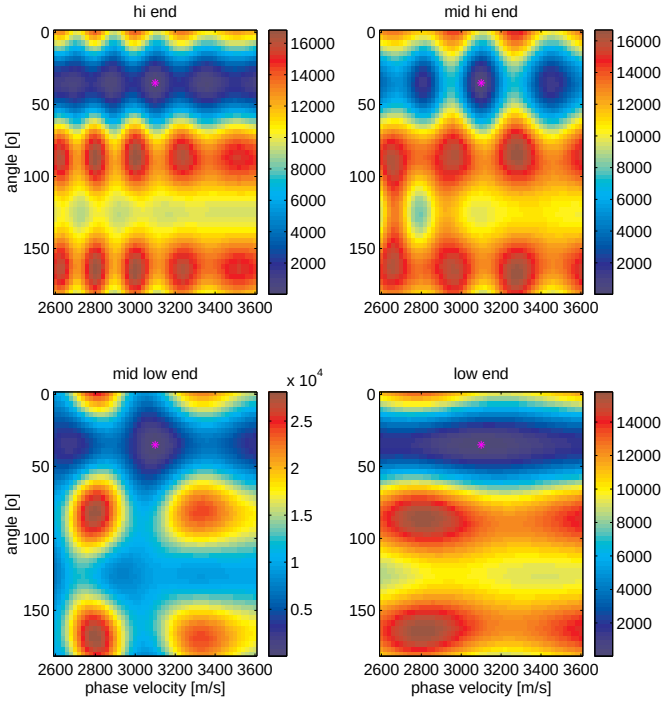

Figure 4: Objective function surfaces for 4 different frequency bands with one dispersion curve held at the correct values.

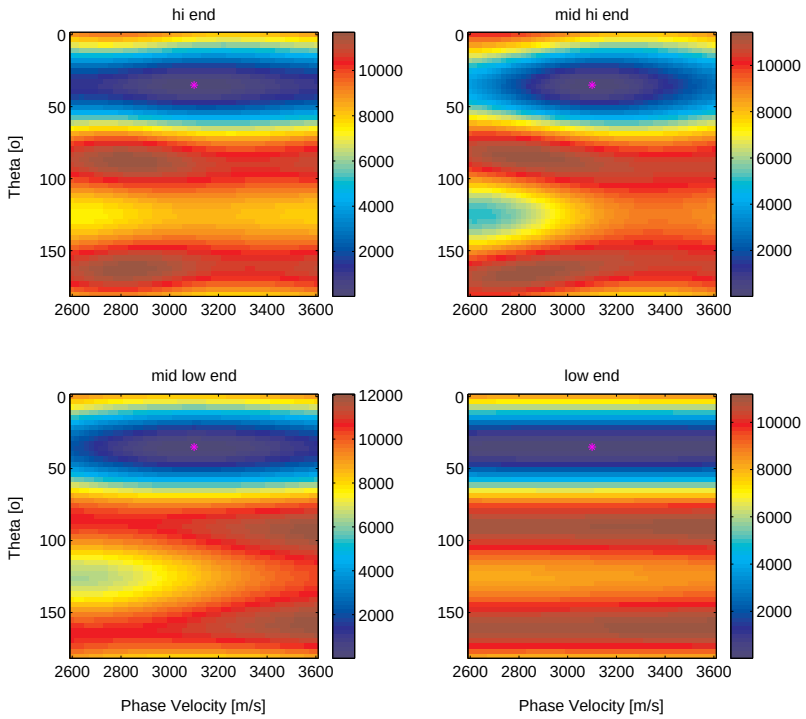

Figure 5: Objective function surfaces for 4 different frequency bands with one dispersion curve held at the correct values and zero offset to the first receiver.

It is clear from figure 5, where the data were created using zero offset, that without this phase wrap, the objective function space is reduced to one smooth minimum. Unfortunatley this phase wrap around cannot be removed from the data, if anisotropy is present, by simply subtracting the phase at the first receiver from each of the wave forms. Hypothetically if the source was positioned with the first receivers at distance z_1 and fired in the x-direction, the recorded signal for the cross-line components at distance z_1 would be zero. For a signal to be recorded at the cross-lines the wave must have propagated some distance. If the phase at the z_1 receiver is just subtracted out from all of the waveforms, the effects of the rotation through the offset have not been removed, and the data have been corrupted making inversion for the shear velocities impossible. This means that an inversion using real data must be back propagated to the source.

The slant of the minima in figures 3 and 2 is due to a correlation between the fast and slow velocity modes. When inverting the data, the objective funtion is looking to find the values of v_f and v_s that back propagate the data to the source function. Although only one choice for each of these dispersion curves will give the correct answer, there can be some trade off between the two modes. In other words, if the inversion chooses the fast mode to be a little slower and the slow mode to be a little faster, there is still a good match of the source functions. This trade off is intrinsic to the objective function, however by using all possible receiver pairs the length of the correlation is reduced. If the same figure were shown for just one reciever pair, the correlation would stretch; conversely, if there were more than 8 pairs of recievers, there would be a shrinking of the minimum in the diagonal direction. Figure 1 shows the spectrum of the synthetic data (the black curve), and from the values on the colourbars on 2 it is clear that the frequencies with higher spectral content have a greater influence on the value of the objective function. For the high and low frequency bands where the spectrum has less magnitude the contribution to the objective function is less. This fact has important consequences for the inversion as the results are likely to be inaccurate where the spectrum has lower magnitude.

3 Results

In this section we present some results from real cross-dipole data from a well in Venezuela. We compare three methods; the joint inversion, simple frequency domain Alford rotation followed by Prony's method and, simple frequency domain Alford rotation followed by a back propagation scheme which inverts each frequncy individually. The simple frequency domain rotation scheme is similar to that of the joint inversion but is calculated without taking into acount the effects of dispersion. Figures 8, 6 and, 12 show reasonable agreement between the three results for depths of 7000, 7500, 6700 and, 8000 ft. Below each inversion result is a calculation of semblance from the data after rotation onto the fast and slow axes. (Figures 7, 9,11 and, 13. The maximum contour corresponds to the velocity of coherrent energy in the waveforms. Table 1 shows the angle calculted by the joint inversion, the angle calculated by the simple frequency domain alford rotation, the difference betwwen these two inversions and, the difference in shear mode velocities taken from semblance of the rotated data. There is a correlation between the depths that have the least anisotopy and the uncertainty in the angle.

Depth ft	Joint Inversion degrees	Simple Inversion degrees	difference degrees	Difference in velocities from fast and slow modes m/s (from semblance)
6700	39	27	12	250
7000	57	59	2	500
7500	57	56	1	700
8000	49	43	6	400

Table 1: Angle between fast plane and tool x-axis for joint inversion and simple angle inversion

4 Conclusion

We have shown a method for the joint inversion of cross-dipole acoustic tool data presented the results for some real data. Whilst the inversion gives a good estimate of azimuthal angle the dispersion relationships can be difficult to invert in this manner for due to phase wrap around between the source and first receiver.

5 Acknowledgements

This work was supported by the Earth Resources Laboratory Founding Members and by the Earth Resources Laboratory Borehole Acoustics and Logging Consortium.

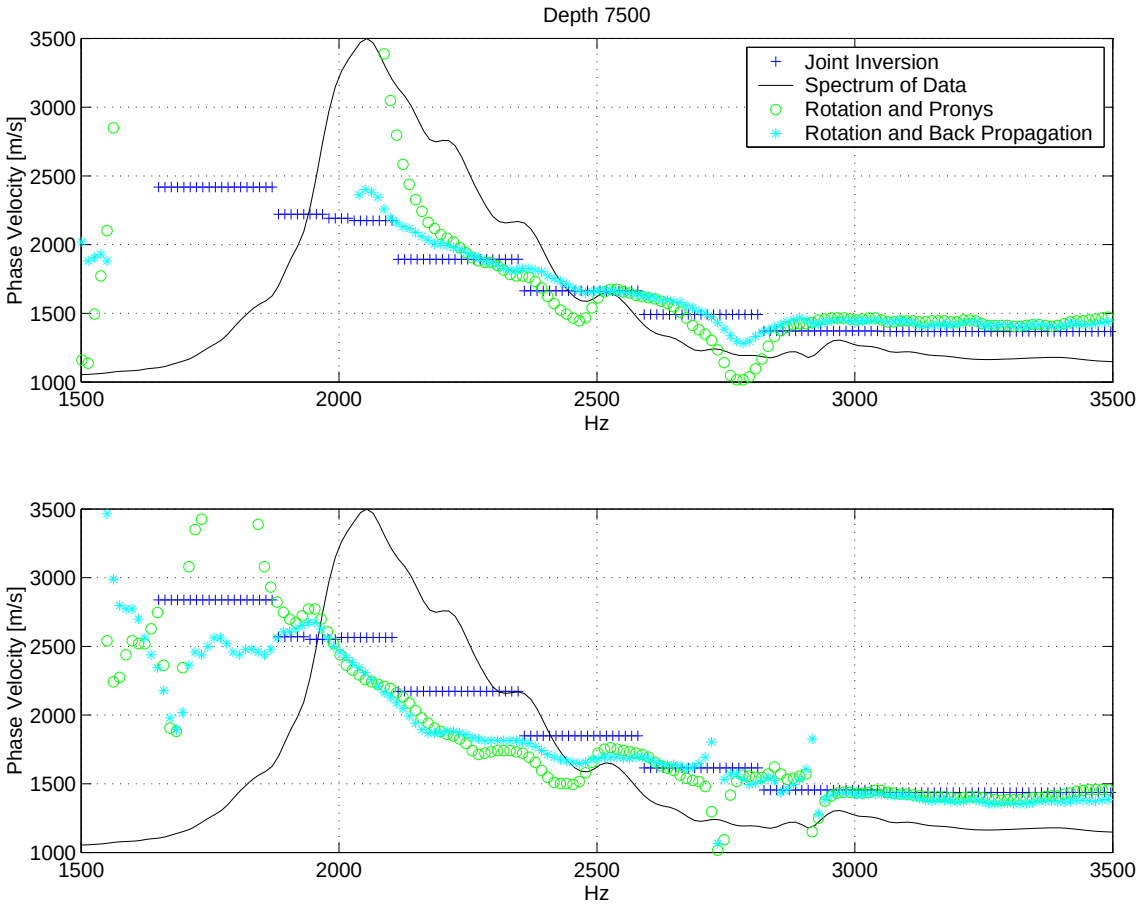

Figure 6: Dispersion analysis results for depth 7500ft.

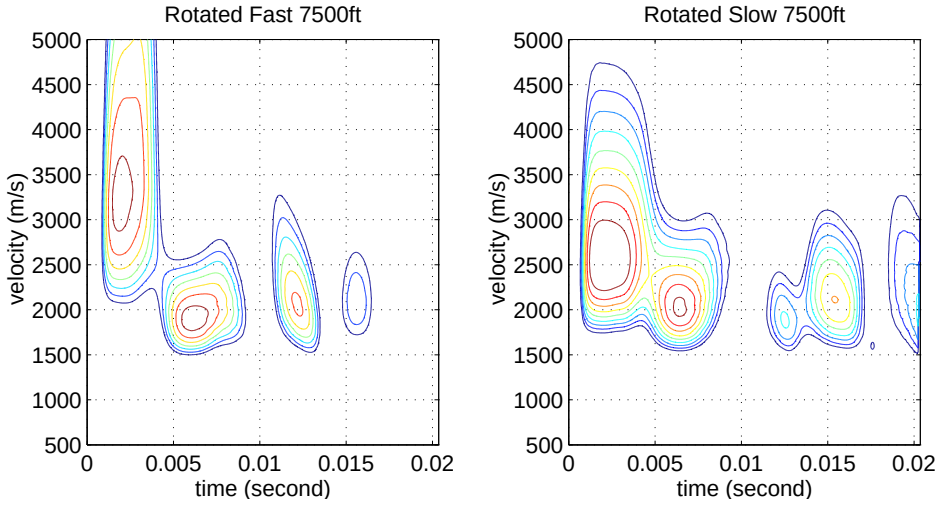

Figure 7: Semblance analysis results for rotated data at depth 7500ft.

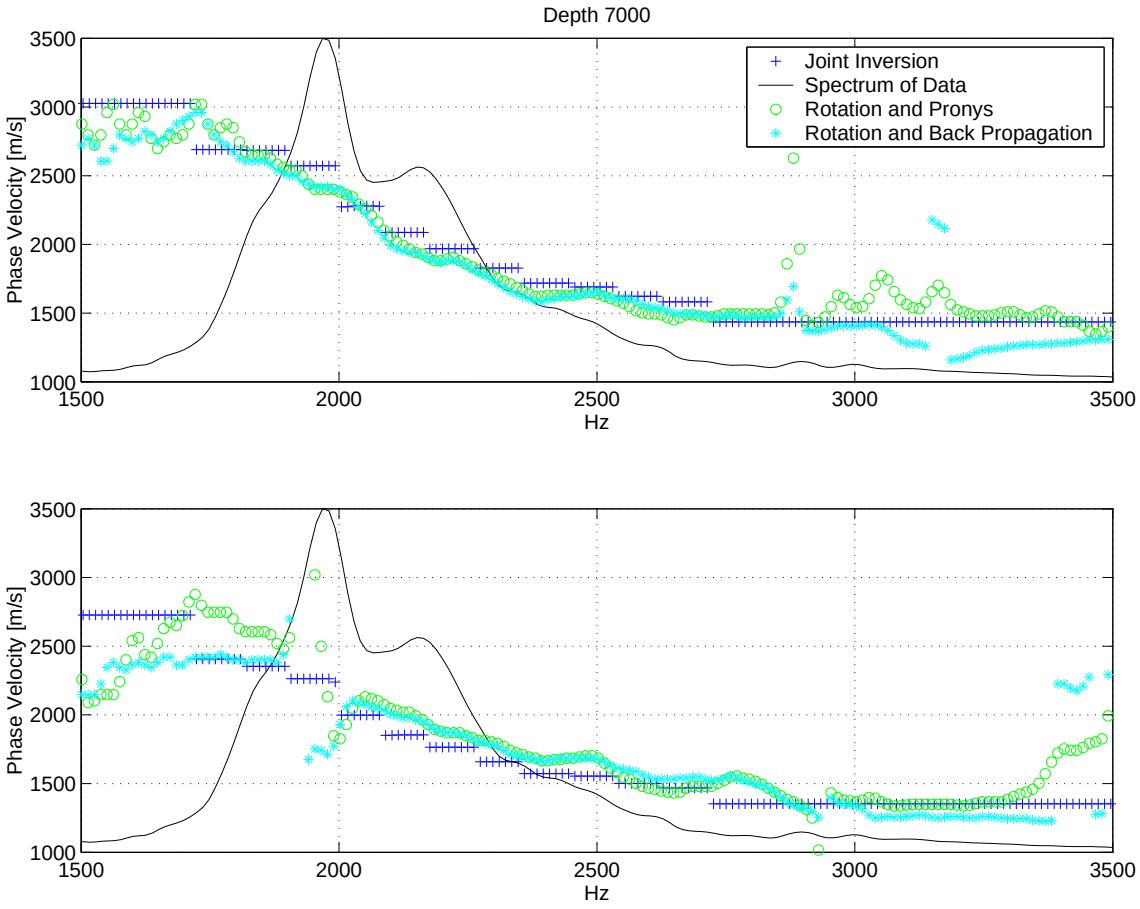

Figure 8: Dispersion analysis results for depth 7000ft.

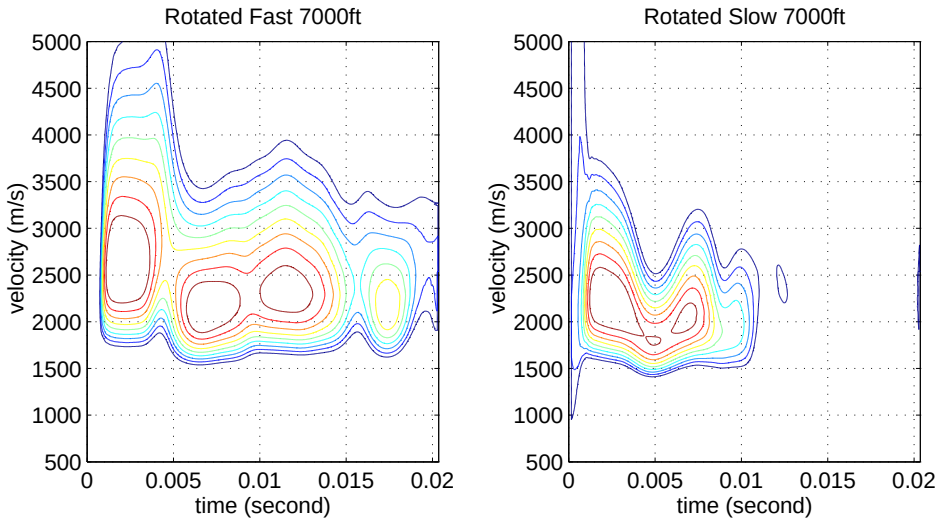

Figure 9: Semblance analysis results for rotated data at depth 7000ft.

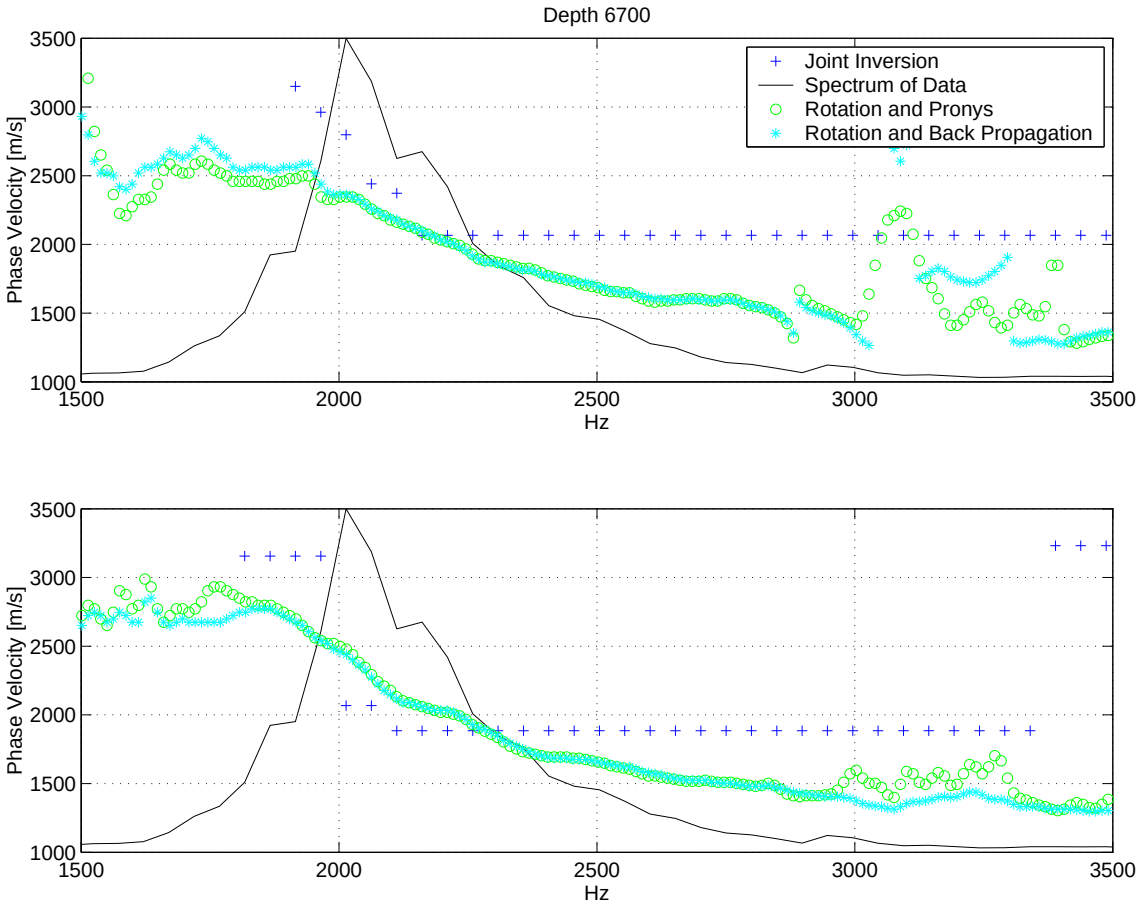

Figure 10: Dispersion analysis results for depth 6700ft.

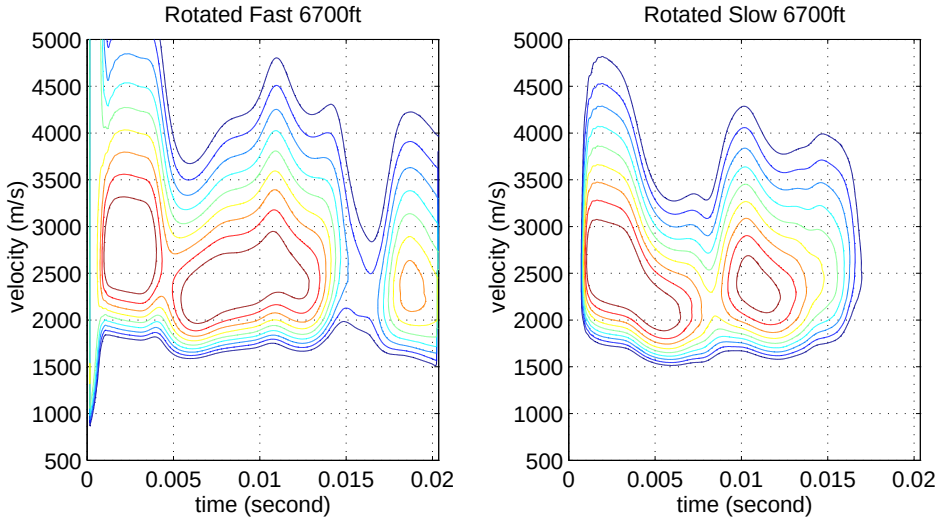

Figure 11: Semblance analysis results for rotated data at depth 6700ft.

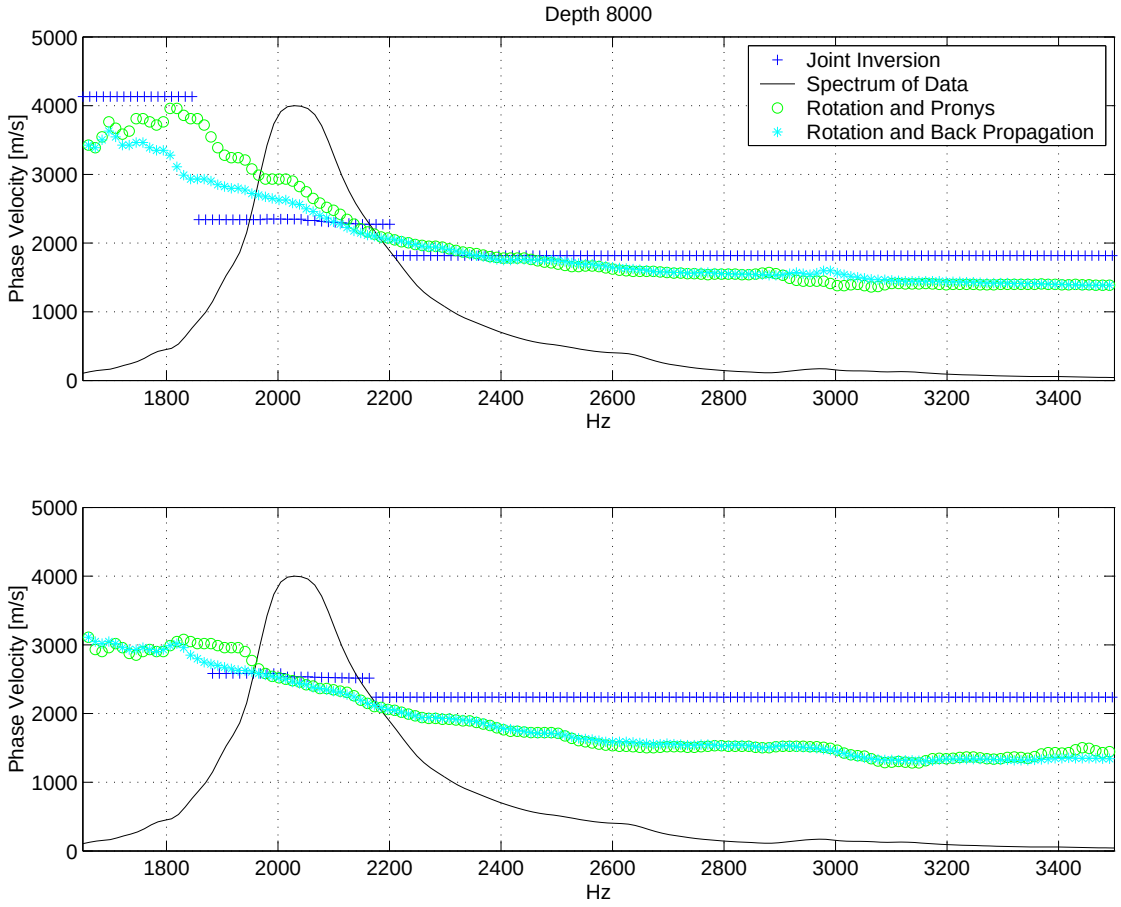

Figure 12: Dispersion analysis results for depth 8000ft.

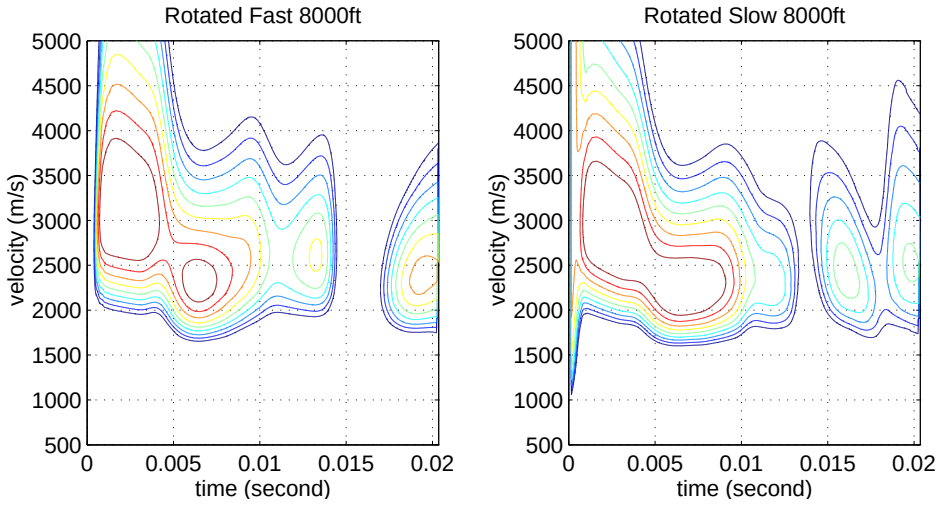

Figure 13: Semblance analysis results for rotated data at depth 8000ft.

References

Alford, R. M. (1986). Shear data in the presence of azimuthal anisotropy. In *Expanded Abstracts*, pages 476–479. Soc. Expl. Geophys.

Huang, X. (1998). A study of tectonic stresses in the earth using standard acoustic logging. Technical report, MIT.

Huang, X., Burns, D. R., and Toksoz, M. N. (1998). Dispersion analysis of cross-dipole data. In *Earth Resources Laboratory MIT Consortia*.

Kimball, C. V. (1998). Shear slowness measurement by dispersive processing of the borehole flexural mode. *Geophysics.*, 63(2):377–344.

Kurkijian, A. L. and Chan, S.-K. (1986). Acoustic multipole sources in fluid-filled boreholes. *Geophysics*, 51(1):148–163.

Sinha, B. K. and Kostek, S. (1996). Stress-induced azimuthal anisotropy in borehole flexural waves. *Geophysics*, 61(6):1899–1907.

Sinha, B. K., Norris, A. N., and Chan, S.-K. (1994). Borehole flexural modes in anisotropic formations. *Geophysics*, 59(7):1037–1052.

Tang, X. and Chunduru, R. K. (1999). Simultaneous inversion of formation shear-wave anisotropy parameters from cross-dipole acoustic-array waveform data. *Geophysics*, 64(5).

Tang, X. M., Reiter, E. C., and Burns, D. R. (1995). A dispersive-wave processing technique for estimating formation shear velocity from diplole and stonely waveforms. *Geophysics*, 60(1):19–28.

Tatham, R. H., Matthews, M. D., Sekharan, K. K., Wade, C. J., and Liro, L. M. (1992). A physical model study of shear wave splitting and fracture intensity. *Geophysics.*, 57(4):647–652.

Tichelaar, B. W. and Hatchell, P. J. (1997). Inversion of 4-c borehole flexural waves to determine anisotropy in a fractured carbonate reservoir. *Geophysics.*, 62(5):1432–1441.

A Appendix

A.1 Cross-Dipole Data

The cross-dipole tool belongs to the family of wireline acoustic tools. It is used primarily to estimate acoustic velocties as a function of radial position in slow formations, (i.e. those whose shear velocity is less than the borehole fluid velocity). Although tool design varies from company to company, all tools have similar general features and consist of two pairs of dipole sources and eight pairs of dipole receivers. The dipole acoustic transducer source pairs are oriented orthogonally on the tool, one pair along the x direction and one along the y direction. The transducer receivers are similarly oriented with the first pair having a large offset from the source and subsequent receivers being evenly distributed with a separation of aproximately 15 cm. (Figure 14 shows a cartoon of a generic cross-dipole tool). This source receiver configuration permits a directional measurement of the formations's acoustic response. The two sources fire separately, and after each excitation the receivers in both the x and y direction record the formation response. This recording results in 4 arrays of 8 (the number of receivers) traces, X source to X receiver referred to as XX, X source to Y receiver referred to XY, and similarly for YX and YY.

When the medium is excited with a dipole source, a set of axisymmetric borehole-guided modes and refracted shear and compressional waves are formed. The guided modes of lowest cut-off frequency, known as flexural modes, are polarized in the x-y plane perpendicular to their direction of propagation that is along the z-axis. If the medium is anisotropic, the flexural wave motion splits into a fast and slow component dependent on the directional velocities of the rock and the frequency component of the excitation. When

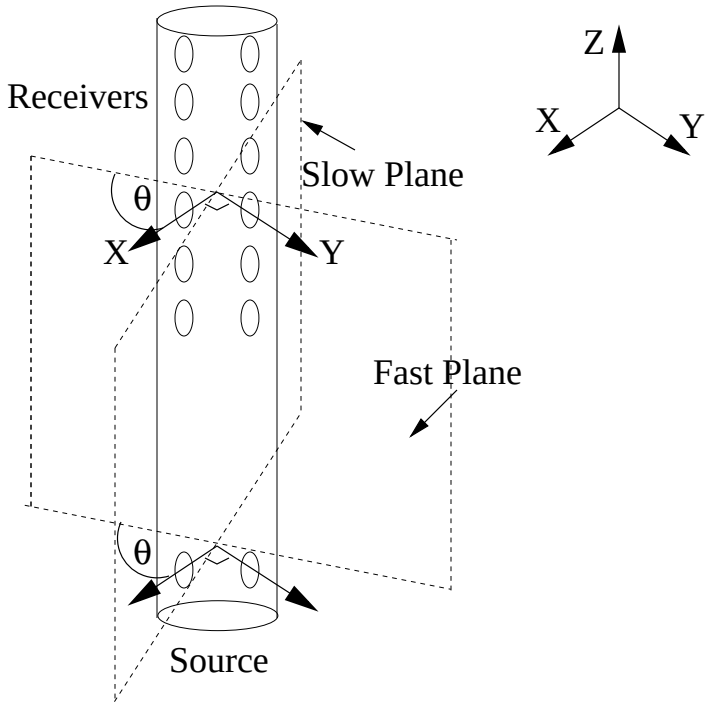

Figure 14: Schematic of generic Cross-Dipole tool.

the source transducer pair oriented along the x-axis is excited, the displacement vector of the flexural wave generated is also in the x direction. The fast and slow axes of the formation make an angle θ with respect to the x and y axes so that the displacement vector has projections $\cos\theta$ and $\sin\theta$ on the fast and slow directions, respectively. The fast and slow flexural waves then propagate with their respective (frequency dependent) velocities and are recorded at the receivers. Since the receivers are also oriented along the x and y axes, the displacement measured is a second projection of the fast and slow modes back onto the x and y axes.

Let $S_x(t)$ and $S_y(t)$ represent the source excitation functions for the x and y oriented dipoles, and let $s_x(\omega)$ and $s_y(\omega)$ be their fourier transforms. Also let $g_f^{(n)}(\omega)$ and $g_s^{(n)}(\omega)$ be the formation propagation function from the source to the n^{th} receiver, i.e.,

$$g_f^{(n)}(\omega) = \exp\{i\frac{\omega}{v_f(\omega)}z_n\} \quad (5)$$

$$g_s^{(n)}(\omega) = \exp\{i\frac{\omega}{v_s(\omega)}z_n\} \quad (6)$$

where $v_f(\omega)$ and $v_s(\omega)$ are the fast and slow frequency dependent phase velocities, respectively, and z_n is the distance from the source to the nth receiver. The signals recorded by the cross dipole tool are therefore given by

$$
\begin{aligned}
xx_n(\omega) &= g_f^{(n)}(\omega)s_x(\omega)\cos^2\theta + g_s^{(n)}(\omega)s_x(\omega)\sin^2\theta && (7)\\
xy_n(\omega) &= [g_f^{(n)}(\omega)s_x(\omega) - g_s^{(n)}(\omega)s_x(\omega)]\cos\theta\sin\theta && (8)\\
yx_n(\omega) &= [g_f^{(n)}(\omega)s_y(\omega) - g_s^{(n)}(\omega)s_y(\omega)]\cos\theta\sin\theta && (9)\\
yy_n(\omega) &= g_f^{(n)}(\omega)s_y(\omega)\sin^2\theta + g_s^{(n)}(\omega)s_y(\omega)\cos^2\theta. && (10)\\
& && (11)
\end{aligned}
$$

Assuming the same source function for both the x and y transducers, $s_x(\omega) = s_y(\omega) = s(\omega)$, and letting $f_n(\omega) = g_f^{(n)}s(\omega)$ and $s_n(\omega) = g_s^{(n)}s(\omega)$, we can now represent equations 7 to 11 in matrix form

$$
\begin{pmatrix} xx_n(\omega) & xy_n(\omega) \\ yx_n(\omega) & yy_n(\omega) \end{pmatrix} = \begin{pmatrix} \cos\theta & -\sin\theta \\ \sin\theta & \cos\theta \end{pmatrix} \begin{pmatrix} f_n(\omega) & 0 \\ 0 & s_n(\omega) \end{pmatrix} \times \begin{pmatrix} \cos\theta & \sin\theta \\ -\sin\theta & \cos\theta \end{pmatrix}. \quad (12)
$$

(13)

A.2 Rotation

We can use equation 13 to create synthetic waveforms for a given source function and dispersion relations. Figures 15 and 16 show the difference between the borehole flexural mode recorded with a tool whose x and y axes are at an angle $\theta = 25^o$ with the formation fast and slow axes, and the borehole flexural mode recorded with a tool which is aligned with the formation fast and slow axes. In matrix terms, if the tools and formation axes are aligned, the diagonal components of equation 13 are maximized and the off diagonal components vanish.

We can invert 13

$$
\begin{pmatrix} f_n(\omega) & 0 \\ 0 & s_n(\omega) \end{pmatrix} = \begin{pmatrix} \cos\theta & \sin\theta \\ -\sin\theta & \cos\theta \end{pmatrix} \begin{pmatrix} xx_n(\omega) & xy_n(\omega) \\ yx_n(\omega) & yy_n(\omega) \end{pmatrix} \times \begin{pmatrix} \cos\theta & -\sin\theta \\ \sin\theta & \cos\theta \end{pmatrix}, \quad (14)
$$

which gives the fast and slow propagation functions as

$$
\begin{aligned}
f_n(\omega) &= xx_n(\omega)\cos^2\theta + [xy_n(\omega) + yx_n(\omega)]\sin\theta\cos\theta + yy_n(\omega)\sin^2\theta && (15)\\
s_n(\omega) &= xx_n(\omega)\sin^2\theta - [xy_n(\omega) + yx_n(\omega)]\sin\theta\cos\theta + yy_n(\omega)\cos^2\theta. && (16)
\end{aligned}
$$

Aditionally, it is easy to see from equations 15 and 16 that if $\theta = 90^o$ or 0^o there will be no $xy_n(\omega)$ or $yx_n(\omega)$ dependence.

A.3 Propagation

Next, the effects of propagation through the formation are undone. Figure 17 shows the data from Figure 16 after the propagation has been undone. If the correct dispersion relation is used (i.e., each frequency component is back propagated at the correct velocity), only the source function remains at each reciever on the inline arrays, and since the correct rotation has been applied, there is no signal on the crossline arrays.

Remembering that $f_n(\omega) = g_f^{(n)}s(\omega)$ and $s_n(\omega) = g_s^{(n)}s(\omega)$, we can write equation 14 as,

$$
\begin{pmatrix} s(\omega) & 0 \\ 0 & s(\omega) \end{pmatrix} = \begin{pmatrix} e^{-i\frac{\omega}{v_f(\omega)}z_n} & 0 \\ 0 & e^{-i\frac{\omega}{v_s(\omega)}z_n} \end{pmatrix} \times \begin{pmatrix} \cos\theta & \sin\theta \\ -\sin\theta & \cos\theta \end{pmatrix} \begin{pmatrix} xx_n(\omega) & xy_n(\omega) \\ yx_n(\omega) & yy_n(\omega) \end{pmatrix} \begin{pmatrix} \cos\theta & -\sin\theta \\ \sin\theta & \cos\theta \end{pmatrix}. \quad (17)
$$

which is valid for any receiver n.

The propagation function has been moved to the righthand side. There is now a complete expression for the rotation and propagation of a source function to each of the array receivers. In other words, if the correct azimuthal angle and dipserion relations, $v_f(\omega)$ and $v_s(\omega)$, are used in equation 17, we recover the source function $s(\omega)$ at every receiver.

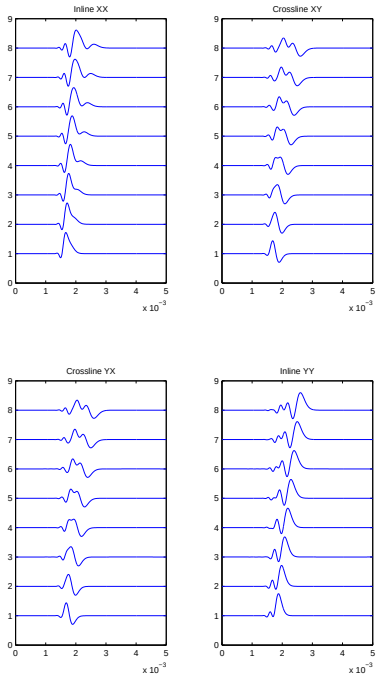

Figure 15: Time series representation of the borehole flexural mode with tool at angle $\theta = 25^o$ with the formation axes.

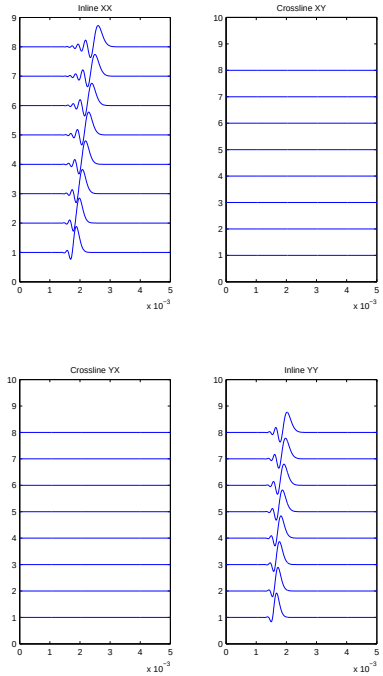

Figure 16: Time series representation of the borehole flexural mode with tool aligned ($\theta = 90^o, 0^o$) with the formation axes.

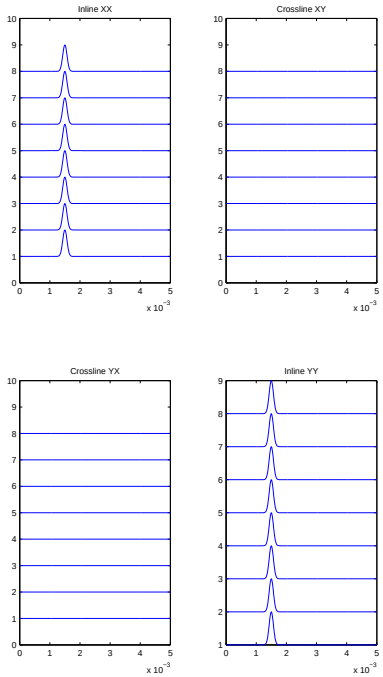

Figure 17: Time series representation of flexural mode after back propagation with the correct dispersion relation.